https://doi.org/10.1016/j.apm.2018.11.046

Theoretical analysis of Rayleigh-Taylor instability on a spherical droplet in a gas stream

Yikai Li[1, *], Peng Zhang[2, *], Ning Kang[1]

1. School of Mechanical Engineering, Beijing Institute of Technology, Beijing 100081, China
2. Department of Mechanical Engineering, the Hong Kong Polytechnic University, Hung Hom, Hong Kong

Abstract: A linear analysis of the Rayleigh-Taylor (R-T) instability on a spherical viscous liquid droplet in a gas stream is presented. Different from the most previous studies in which the external acceleration is usually assumed to be radial, the present study considers a unidirectional acceleration acting on a spherical droplet with arbitrary initial disturbances and therefore can provide insights into the influence of R-T instability on the atomization of spherical droplets. A general recursion relation coupling different spherical modes is derived and two physically prevalent limiting cases are discussed. In the limiting case of inviscid droplet, the critical Bond numbers to excite the instability and the growth rates for a given Bond number are obtained by solving two eigenvalue problems. In the limiting case of large droplet acceleration, different spherical modes are asymptotically decoupled and an explicit dispersion relation is derived. For given Bond number and Ohnesorge numbers, the critical size of stable droplet, the most-unstable mode and its corresponding growth rate are determined theoretically.

Keywords: Rayleigh-Taylor instability, spherical droplet, linear analysis, non-radial acceleration, secondary atomization

* Corresponding author.
E-mail address: liyikai@bit.edu.cn (Y. Li), pengzhang.zhang@polyu.edu.hk (P. Zhang)

1. Introduction

Spray combustion is widely used in many engineering applications such as aircraft engines, automotive engines and oil-fired furnaces **[1, 2]**. The combustion and emission performance strongly depend on the spray characteristics, which is in turn affected by microscopic processes of liquid droplet atomization. After the fuel spray emanates into the combustion chamber, liquid masses (sheets, filaments and droplets) of relatively large sizes are first formed by primary breakup, followed by their secondary atomization to produce droplets of smaller sizes **[3-5]**.

Secondary atomization of liquid droplets results from their interaction with the surrounding gas flow. It is found that different atomization mechanisms occur for different relative velocity between droplets and the gas flow **[6-9]**. In modern aircraft and automotive engines, the gas flow speed in the combustion chamber is usually rather high, and therefore acts a large acceleration on the droplets. In such a scenario, the Rayleigh-Taylor (R-T for short hereinafter) unstable waves form on the windward surface of the liquid drops, develop their amplitudes, and eventually breakup the droplets **[10]**. Such a mechanism for droplet secondary atomization in high-speed gas flow is also referred to as the "catastrophic atomization" **[8, 11]**.

R-T instability, which is excited on a liquid-gas interface where an acceleration is applied from the light fluid to the heavy, has been extensively observed and applied in many scientific and industrial fields **[12-14]**. It was first discovered by Rayleigh **[15]** for a heavy fluid lying on a lighter one under gravity and then extended to accelerated

fluids by Taylor **[16]**, who derived a dispersion relation through a linear analysis for an ideal flow without considering capillary force. The destabilizing effects of fluid viscosity and surface tension force on R-T instability were further studied by Bellman and Pennington **[17]**. Since then, extensive investigations have been conducted to study the detailed dynamics of R-T instability **[14, 18, 19]**.

In spite of these worthy works offering good insights into the R-T instability, most of the previous studies focus on the planar configuration. The R-T instability on a curved interface is believed to reveal different features. There are only a few studies devoted to the R-T instability at spherical interfaces in the fields of nuclear fusion and gas bubble stability **[20, 21]**, in which the acceleration is usually assumed to be along the radial direction (spherically symmetric) **[22]**. As a result, most of the models accounting for the atomization of liquid droplets caused by R-T instability, which have been widely applied in the spray combustion simulation, are based on the flat surface assumption **[10, 11]** and obviously deviates from the realistic condition.

With a simplified theory based on viscous potential flow, Joseph et al. **[10]** studied the breakup of a viscous droplet at high Bond number (*Bo*) and predicted the maximum diameter for an unconditionally stable droplet by considering the windward of droplet as a flat surface. Harper et al. **[23]** have theoretically studied the R-T instability of an inviscid spherical droplet under a uniform acceleration by using a linear analysis, in which the variation of acceleration along the polar angle couples different spatial modes, and a recursion relation was proposed to compute the growth rate. They obtained the

minimum *Bo* to excite the zonal instability and showed that the droplet is unstable to the disturbances whose wavelengths are larger than a critical value being proportional to $Bo^{1/2}$. This result was experimentally validated by Simpkins and Bales **[24]**.

Regardless of the valuable conclusions for the breakup of spherical drops caused by R-T instability, some important aspects remain unclear due to the assumptions made in these studies. In the work of Harper et al. **[23]**, the initial disturbance imposed on a spherical droplet surface is assumed to be axisymmetric and thus the discussions are restricted to the zonal harmonics. However, the general arbitrary disturbance in the realistic condition is a sum of the spherical harmonics with different coefficients. The dynamic response to the disturbance of meridional modes may also affect the atomization process significantly. In addition, Harper et al. **[23]** also neglected the liquid viscosity, which has been shown to affect the linear growth rate for the planar R-T instability. Joseph et al. **[10]** did a linear analysis to the viscous R-T instability for explaining their experiments for a spherical liquid droplet, but the analysis was based on the approximation of flat windward droplet surface. To understand the breakup process of a liquid droplet in a gas stream under more realistic situations, we studied the dynamic response of a spherical viscous liquid droplet under a uniform acceleration to arbitrary (non-axisymmetric) disturbances. Such a problem, to our knowledge, has not been addressed in the literature.

The rest of this paper is organized as follows. In Section 2, a spherical R-T instability for a viscous liquid droplet with arbitrary initial disturbances is first

mathematically formulated. In Section 3, the general solution to the formulation is derived, yielding a set of difference equations with the coefficient matrix being a function of both zonal and meridional modes. In Sections 4 and 5, the solutions in the inviscid and large-mode number limits are discussed. Finally, the results of this study are summarized in Section 6.

2. Mathematical model

The present problem of interfacial dynamics occurring on the spherical liquid droplet placed in a gaseous flow of high speed can be simplified as an initially stationary viscous and incompressible spherical liquid droplet (of density ρ_1 and radius r_0) suddenly accelerated in an initially quiescent medium of inviscid and incompressible gas (of density $\rho_2 < \rho_1$), as shown in Fig. 1. This approximation requires that the characteristic time for developing the R-T unstable waves is too short to accelerate the droplet to a significant velocity. The Kelvin-Helmholtz (K-H for short hereinafter) instability **[25]** triggered by the tangential velocity difference between two phases on the interface is apparently present in the realistic situation. To avoid unnecessary complexity added to the present formation, the K-H instability is not considered here but certainly merits future study for its coupling with the R-T instability. Different from most of the previous studies on the spherical R-T instability, the direction of acceleration A on the liquid droplet is uniform instead of an unrealistic radial one. The surface tension coefficient α is assumed to be constant all over the interface, implying

that the effects of temperature and surfactant are not considered here. The gravitational acceleration, g, is neglected because of the assumption of $A \gg g$ being in accordance with the typical situation in aircraft or automotive engines.

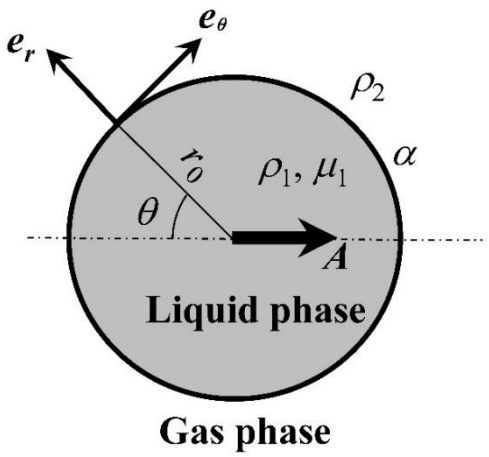

Fig. 1 Schematic of the non-radial spherical R-T instability.

In the reference frame attached to the liquid droplet, the linearized governing equations are

$$\nabla \bullet \boldsymbol{u}_i = 0 \tag{1}$$

$$\frac{\partial \boldsymbol{u}_i}{\partial t} = -\frac{1}{\rho_i}\nabla p_i + \nu_i \nabla^2 \boldsymbol{u}_i - \boldsymbol{A}, \tag{2}$$

where the subscripts i=1, 2 represent the physical quantities for the liquid and gas phase, respectively; $\boldsymbol{u_i}$ is the perturbed velocity vector, p_i the pressure, $\nu_i = \mu_i / \rho_i$ the kinematic viscosity ($\nu_2 = 0$), and $\boldsymbol{A} = -A\cos\theta \boldsymbol{e}_r + A\sin\theta \boldsymbol{e}_\theta = -\nabla\left(gr\cos\theta\right)$. As shown in Fig. 1, $\boldsymbol{e}_r$ and $\boldsymbol{e}_\theta$ are the unit vector along the radial and polar direction in the spherical coordinate system (r, θ, φ).

The interfacial deformation displacement is denoted by $\eta(\theta, \varphi, t)$ and the linearized kinematic condition on the droplet surface is given by

$$\frac{\partial \eta}{\partial t} = u_{1r}\big|_{r=r_0+\eta} = u_{2r}\big|_{r=r_0+\eta}, \tag{3}$$

where u_{ir} (i=1,2) is the radial component of the velocity vector $\boldsymbol{u}_i$.

The balance of normal stress across the interface gives **[26]**

$$\left[\boldsymbol{e}_r \bullet \boldsymbol{\sigma} \bullet \boldsymbol{e}_r\right]_1^2 = \alpha \nabla \bullet \boldsymbol{e}_r = \alpha\left(\frac{1}{R_a}+\frac{1}{R_b}\right), \tag{4}$$

where $\left[x\right]_1^2 = x_2 - x_1$, $\boldsymbol{e}_\mathbf{r}$ is the unit vector normal to interface directing outwardly from the droplet, $\boldsymbol{\sigma}$ the stress tensor defined by

$$\boldsymbol{\sigma}_i = -p_i \boldsymbol{I} + \mu_i\left[\nabla \boldsymbol{u}_i + \left(\nabla \boldsymbol{u}_i\right)^T\right], \tag{5}$$

and R_a and R_b the principle radii of curvature which can be expressed as

$$\frac{1}{R_a}+\frac{1}{R_b} = \frac{2}{r_0} - \frac{1}{r_0^2}\left(2\eta + \nabla_H^2 \eta\right), \tag{6}$$

up to the first order in η **[26]**, where

$$\nabla_H^2 \equiv \frac{1}{\sin\theta}\frac{\partial}{\partial\theta}\left(\sin\theta\frac{\partial}{\partial\theta}\right) + \frac{1}{\sin^2\theta}\frac{\partial^2}{\partial\varphi^2} \tag{7}$$

is the horizontal spherical Laplacian operator. With Eqs (5) to (7), the balance equation of the normal stress reduces to

$$p_1\big|_{r=r_0+\eta} - p_2\big|_{r=r_0+\eta} = \frac{2\alpha}{r_0} - \frac{\alpha}{r_0^2}\left(2\eta + \nabla_H^2\eta\right) + 2\mu_1 \left.\frac{\partial u_{1r}}{\partial r}\right|_{r=r_0+\eta}, \tag{8}$$

The tangential stress on the two sides of the interface must satisfies

$$\left[\boldsymbol{n} \bullet \boldsymbol{\sigma} \bullet \boldsymbol{e}_j\right]_1^2 = 0, \tag{9}$$

where $\boldsymbol{e}_j = \boldsymbol{e}_\theta$, $\boldsymbol{e}_\varphi$ represent the unit vectors tangential to the droplet surface towards polar and azimuthal directions, respectively. Since the gas phase is assumed to be inviscid, the balance of the tangential stress across the interface gives

$$\sigma_{r\theta} = \mu_1\left(\frac{1}{r}\frac{\partial u_{1r}}{\partial\theta} - \frac{u_{1\theta}}{r} + \frac{\partial u_{1\theta}}{\partial r}\right) = 0 \tag{10}$$

and

$$\sigma_{r\varphi}=\mu_1\left(\frac{1}{r\sin\theta}\frac{\partial u_{1r}}{\partial\varphi}-\frac{u_{1\varphi}}{r}+\frac{\partial u_{1\varphi}}{\partial r}\right)=0\,. \tag{11}$$

Instead of the Legendre function expansion adopted by Harper et al. **[23]** under the axisymmetric assumption ($\partial/\partial\varphi=0$), we expanded $\eta(\theta,\varphi,t)$ as

$$\eta\left(\theta,\varphi,t\right)=e^{-\zeta t}\sum_{l=2}^{+\infty}\sum_{m=0}^{l}\eta_l^m Y_l^m\left(\theta,\varphi\right) \tag{12}$$

with the spherical harmonics $Y_l^m\left(\theta,\varphi\right)=P_l^m\left(\cos\theta\right)e^{im\varphi}$, where η_l^m ($\eta_0^0=\eta_1^0=\eta_1^1=0$) is the corresponding coefficient and ζ the growth rate. The surface displacement grows to diverge if $\mathrm{Re}\left(\zeta\right)<0$. Eqs. (1)~(12) constitute an eigenvalue problem, the solution to which gives the dispersion relation between the growth rate ζ and the mode number (*l*, *m*) and flow parameters.

3. General solution

For the liquid phase, the momentum equation (2) reduces to

$$\frac{\partial\boldsymbol{u}_1}{\partial t}=-\frac{1}{\rho_1}\nabla p_1-\nu_1\nabla^2\times\boldsymbol{u}_1-\boldsymbol{A}\,. \tag{13}$$

by using the equation $\nabla\times\nabla\times\boldsymbol{u}_1=\nabla\left(\nabla\bullet\boldsymbol{u}_1\right)-\nabla^2\boldsymbol{u}_1$ and the continuity equation (1). The velocity vector $\boldsymbol{u}_1$ can be considered as the sum of the irrotational component $\nabla\phi_1$ and the rotational component $\boldsymbol{\psi}_1$, i.e., $\boldsymbol{u}_1=\nabla\phi_1+\boldsymbol{\psi}_1$, and thus Eq. (13) is decomposed into

$$\nabla^2\phi_1=0 \tag{14}$$

$$p_1=-\rho_1\frac{\partial\phi_1}{\partial t}+\rho_1 Ar\cos\theta+C_1 \tag{15}$$

$$\nabla \bullet \boldsymbol{\psi}_1 = 0 \tag{16}$$

$$\frac{\partial \boldsymbol{\psi}_1}{\partial t} + \nu_1 \nabla^2 \times \boldsymbol{\psi}_1 = 0\,, \tag{17}$$

where C_1 is an integral constant.

Considering that ϕ_1 does not diverge at r =0, the general solution to Eq. (14) in the spherical coordinate is

$$\phi_1(r,\theta,\varphi,t) = e^{-\zeta t}\sum_{l=2}^{+\infty}\sum_{m=0}^{l} B_l^m r^l Y_l^m\,, \tag{18}$$

where the coefficient B_l^m is to be determined by the boundary conditions. Using the method of Chandrasekhar **[27]** to solve Eqs. (16) and (17), we obtained the three components of $\boldsymbol{\psi}_1$ as

$$\left.\begin{aligned}
\psi_{1r}(r,\theta,\varphi,t) &= e^{-\zeta t}\sum_{l=2}^{+\infty}\sum_{m=0}^{l}\frac{l(l+1)}{r^2}\Psi_{1l}^m(r)Y_l^m \\
\psi_{1\theta}(r,\theta,\varphi,t) &= e^{-\zeta t}\sum_{l=2}^{+\infty}\sum_{m=0}^{l}\frac{1}{r}\frac{d\Psi_{1l}^m(r)}{dr}\frac{\partial Y_l^m}{\partial\theta} \\
\psi_{1\varphi}(r,\theta,\varphi,t) &= e^{-\zeta t}\sum_{l=2}^{+\infty}\sum_{m=0}^{l}\frac{1}{r\sin\theta}\frac{d\Psi_{1l}^m(r)}{dr}\frac{\partial Y_l^m}{\partial\varphi}
\end{aligned}\right\} \tag{19}$$

with $\Psi_{1l}^m(r) = D_l^m r^{1/2} J_{l+1/2}(qr)$, where D_l^m is a coefficient to be determined below, and $J_{l+1/2}$ is the spherical Bessel function of order l+1/2 and $q=\sqrt{\zeta/\nu_1}$.

Inserting Eqs. (18) and (19) into boundary conditions (3), (10) and (11), we obtained the expressions for the coefficients B_l^m and D_l^m:

$$\left.\begin{aligned}
B_l^m &= -\frac{\eta_l^m \zeta}{l r_0^{l-1}}\left[1+\frac{2\left(l^2-1\right)}{2xQ_{l+1/2}(x)-x^2}\right] \\
D_l^m &= \frac{2(l-1)\eta_l^m \zeta r_0^{3/2}}{l\left[2xJ_{l+3/2}(x)-x^2 J_{l+1/2}(x)\right]}
\end{aligned}\right\}, \tag{20}$$

where $Q_{l+1/2}(x) = J_{l+3/2}(x)/J_{l+1/2}(x)$ and $x=qr_0$.

The pressure on the liquid side of the interface can be attained by substituting Eqs. (18) and (20) into Eq. (15):

$$p_1\big|_{r=r_0+\eta} = -e^{-\zeta t}\sum_{l=2}^{+\infty}\sum_{m=0}^{l}\frac{\rho_1\zeta^2 r_0}{l}\left[1+\frac{2\left(l^2-1\right)}{2xQ_{l+1/2}\left(x\right)-x^2}\right]\eta_l^m Y_l^m + \rho_1 A\cos\theta\left(r_0+e^{-\zeta t}\sum_{l=2}^{+\infty}\sum_{m=0}^{l}\eta_l^m Y_l^m\right)+C_1. \tag{21}$$

Considering that the presence of $\cos\theta$ in the second term on the right-hand side of Eq. (21) makes the equation inhomogeneous in space and couples the different modes of spherical harmonics, we have

$$\begin{aligned}\cos\theta\sum_{l=2}^{+\infty}\sum_{m=0}^{l}\eta_l^m Y_l^m\left(\theta,\varphi\right) &= \sum_{l=2}^{+\infty}\sum_{m=0}^{l}\eta_l^m e^{im\varphi}\cos\theta P_l^m\left(\cos\theta\right)\\ &= \sum_{l=2}^{+\infty}\sum_{m=0}^{l}\eta_l^m e^{im\varphi}\left[\frac{l-m+1}{2l+1}P_{l+1}^m\left(\cos\theta\right)+\frac{l+m}{2l+1}P_{l-1}^m\left(\cos\theta\right)\right]\\ &= \sum_{l=2}^{+\infty}\sum_{m=0}^{l}\frac{l-m+1}{2l+1}\eta_l^m Y_{l+1}^m+\sum_{l=2}^{+\infty}\sum_{m=0}^{l}\frac{l+m}{2l+1}\eta_l^m Y_{l-1}^m\\ &= \sum_{l=2}^{+\infty}\sum_{m=0}^{l}\frac{l-m}{2l-1}\eta_{l-1}^m Y_l^m+\sum_{l=2}^{+\infty}\sum_{m=0}^{l}\frac{l+m+1}{2l+3}\eta_{l+1}^m Y_l^m,\end{aligned} \tag{22}$$

with which Eq. (21) reduces to

$$p_1\big|_{r=r_0+\eta} = e^{-\zeta t}\sum_{l=2}^{+\infty}\sum_{m=0}^{l}\left\{\frac{\rho_1 A\left(l-m\right)}{2l-1}\eta_{l-1}^m-\frac{\rho_1\zeta^2 r_0}{l}\left[1+\frac{2\left(l^2-1\right)}{2xQ_{l+1/2}\left(x\right)-x^2}\right]\eta_l^m+\frac{\rho_1 A\left(l+m+1\right)}{2l+3}\eta_{l+1}^m\right\}Y_l^m + \rho_1 A r_0\cos\theta+C_1. \tag{23}$$

For the inviscid gas phase which is initially stagnant, a velocity potential ϕ_2 satisfying $\boldsymbol{u}_2=\nabla\phi_2$ is introduced to the continuity equation (1), yielding

$$\nabla^2\phi_2=0. \tag{24}$$

Considering that the velocity does not diverge at $r = \infty$ and the condition (3), we

obtained the solution to Eq. (24) as

$$\phi_2 = e^{-\zeta t}\sum_{l=2}^{+\infty}\sum_{m=0}^{l}\eta_l^m \frac{\zeta r_0}{l+1}\left(\frac{r}{r_0}\right)^{-(l+1)} Y_l^m . \tag{25}$$

Using Eq. (25) and integrating Eq. (2) over r, we have the pressure on the gas side of the interface:

$$p_2\big|_{r=r_0+\eta} = e^{-\zeta t}\sum_{l=2}^{+\infty}\sum_{m=0}^{l}\left[\frac{\rho_2 A(l-m)}{2l-1}\eta_{l-1}^m + \frac{\rho_2\zeta^2 r_0}{l+1}\eta_l^m + \frac{\rho_2 A(l+m+1)}{2l+3}\eta_{l+1}^m\right]Y_l^m$$
$$+ \rho_2 A r_0\cos\theta + C_2, \tag{26}$$

where C_2 is an integral constant.

Substitution of (23) and (26) into Eq. (8) with the identity $\nabla_H^2 Y_l^m = -l(l+1)Y_l^m$ gives

$$e^{-\zeta t}\sum_{l=2}^{+\infty}\sum_{m=0}^{l}\left\{\frac{(\rho_1-\rho_2)A(l-m)}{2l-1}\eta_{l-1}^m\right.$$
$$-\left[\left(\frac{\rho_1}{l}+\frac{\rho_2}{l+1}\right)r_0\zeta^2 + 2\mu_1\zeta\frac{l-1}{lr_0}\left(\frac{(2l+1)x-2l(l+2)Q_{l+1/2}(x)}{2Q_{l+1/2}(x)-x}\right)+\frac{\alpha(l-1)(l+2)}{r_0^2}\right]\eta_l^m$$
$$\left.+\frac{(\rho_1-\rho_2)A(l+m+1)}{2l+3}\eta_{l+1}^m\right\}Y_l^m + (\rho_1-\rho_2)Ar_0\cos\theta + C_1 - C_2 - \frac{2\alpha}{r_0} = 0, \tag{27}$$

in which the coefficients of Y_l^m satisfy

$$\frac{(\rho_1-\rho_2)A(l-m)}{2l-1}\eta_{l-1}^m - \left[\left(\frac{\rho_1}{l}+\frac{\rho_2}{l+1}\right)r_0\zeta^2 + 2\mu_1\zeta\frac{l-1}{lr_0}\left(\frac{(2l+1)x-2l(l+2)Q_{l+1/2}(x)}{2Q_{l+1/2}(x)-x}\right)\right.$$
$$\left.+\frac{\alpha(l-1)(l+2)}{r_0^2}\right]\eta_l^m + \frac{(\rho_1-\rho_2)A(l+m+1)}{2l+3}\eta_{l+1}^m = 0, l = 2,3,\ldots, \tag{28}$$

since the functions $Y_l^m(\theta,\varphi)$ are linearly independent. Solving the difference equation (28) would give the dispersion relation. Note that the growth rate ζ to be derived is a function of both l and m, which will be discussed in detail in the following

sections. This is more general than the axisymmetric spherical R-T instability in which ζ depends only on l **[23]**.

4. Inviscid limit

Eq. (28) is the generalized recursion relation for the spherical R-T instability, which includes the effects of density ratio, liquid viscosity and surface tension. Our focus in this paper is on the atomization of a spherical liquid droplet under uniform accelerations, in which the density of the surrounding gas is usually far smaller than that of the liquid droplet ($\rho_2 \ll \rho_1$). Furthermore, to facilitate the following comparison with the previous studies, we first considered the inviscid case ($\nu_1 = \nu_2 = 0$). Consequently, with the definition of Bond number $Bo = \rho_1 A r_0^2 / \alpha$, which measures the relative importance of the inertial force compared with the capillary force, and dimensionless growth rate $\hat{\zeta} = \zeta / \sqrt{A / r_0}$, Eq. (28) is reduced to

$$\frac{l(l-m)}{2l-1}\eta_{l-1}^{m} - \left[\hat{\zeta}^2 + \frac{l(l-1)(l+2)}{Bo}\right]\eta_l^m + \frac{l(l+m+1)}{2l+3}\eta_{l+1}^{m} = 0, l = 2,3,\ldots, \qquad (29)$$

which degenerates to that obtained by Harper et al. **[23]** for m=0.

In particular, we are interested in two solutions to Eq. (29). The first is to determine the critical Bond number $(Bo_{cr})_i$ to excite the instability (i is the number of excited zonal modes) for a given m-value. Each critical Bond number results in the growth rate $\hat{\zeta} = 0$, which represents a neutral stability state. The second is to determine the dimensionless growth rate $\hat{\zeta}$ for positive real values of Bo and discrete mode numbers (l, m), with which we can obtain the most-unstable mode for a given Bond number in a specified

realistic experimental condition. The procedure to solve these problems for the spherical droplet under uniform acceleration is substantially more complicated than that for the liquid layer **[16]** or the spherical droplet under radial acceleration **[22]** because of the coupled spherical modes, as indicated in Eq. (29).

We first studied the infinite set of critical Bond numbers $(Bo_{cr})_i$, which are usually obtained by interpolating *Bo* between positive and negative values of $\hat{\zeta}$ **[23]**. This approach is rather laborious and not sufficiently accurate. In this study, we alternatively adopted the procedure conventionally used to determine the marginal stability boundary for Faraday instability **[28, 29]**, which can directly give the values of critical Bond numbers $(Bo_{cr})_i$ without invoking any interpolation.

Setting $\hat{\zeta}=0$ in Eq. (29), we obtain

$$\frac{l-m}{(2l-1)(l-1)(l+2)}\eta_{l-1}^{m}+\frac{l+m+1}{(2l+3)(l-1)(l+2)}\eta_{l+1}^{m}=\frac{1}{Bo}\eta_{l}^{m},\ l=2,3,\ldots. \qquad (30)$$

Physically, each critical Bond number $(Bo_{cr})_i$ can be considered as the reciprocal of the *i*-th real and positive eigenvalue of a banded coefficient matrix, **M**, with all the elements being null except $M_{k,k-1}(k=2,3,\ldots)$ and $M_{k,k+1}(k=1,2,\ldots)$. The eigenvalue problem of Eq. (30) is solved numerically by truncating the coefficient matrix above $M_{N,N}$. The eigenvalues of lower orders are converged as the truncation number *N* increases **[23]**. As a result, we can always obtain the critical Bond numbers of interest by setting sufficiently large value of *N*.

With the increase of the meridional mode number *m* ($\geqslant 3$), the lower bound of *l* in the coefficient matrix is increased accordingly due to the constraint $m \leq l$. Table 1

gives the first ten critical Bond numbers $(Bo_{cr})_i$ for m = 0, 1, 2, 3 and 4. It can be seen that the number of unstable modes increases with the increase of Bo for a given value of m. Furthermore, compared with the axisymmetric solution (m = 0) of Harper et al. **[23]**, the present results show that more unstable modes (besides the modes of m = 0) would be excited during the increasing path of Bo. For each Bo that exceeds one critical value $(Bo_{cr})_i$ in Table 1 (and its extension in i- and m-values), an extra unstable spherical mode emerges.

One of our interests in the present linear stability analysis is the lowest critical Bo for different m-values, below which the droplet is unconditionally stable to the corresponding meridional disturbance of m-mode. From Table 1 it is seen that the lowest critical Bo increases as m increases, indicating that the instability of higher meridional mode is more difficult to be excited. The global minimum critical Bo is $(Bo_{cr})_{min}$=11.22, below which no instability occurs on the spherical surface. Note that the viscosity of liquid droplet has no influence on $(Bo_{cr})_i$ because the neutral stability condition, $\hat{\zeta} = 0$, gives rise to the same difference equation (30) for both inviscid and viscous cases.

Table 1 The first ten critical Bond numbers $(Bo_{cr})_i$ for m=0, 1, 2, 3 and 4.

	m = 0	m = 1	m = 2	m = 3	m = 4
i = 1	11.22	11.84	14.53	31.45	53.42
i = 2	38.34	39.13	42.05	66.12	95.36
i = 3	79.43	80.29	83.30	114.37	150.73
i = 4	134.33	135.24	138.31	176.31	219.69
i = 5	203.01	203.96	207.06	251.98	302.33

$i = 6$	285.47	286.43	289.56	341.38	398.67
$i = 7$	381.69	382.67	385.82	444.52	508.73
$i = 8$	491.66	492.66	495.82	561.41	632.52
$i = 9$	615.39	616.40	619.57	692.04	770.06
$i = 10$	752.95	753.96	757.15	836.43	921.34

The critical Bond numbers merely give the number of excited spherical modes but do not provide any information on which modes (l) are excited. This information is the key to construct the secondary atomization model because the leading size of the atomized droplets has been found to be proportional to the surface wavelength corresponding to the most-unstable modes **[30, 31]**. To solve this problem, we need to find the value of the growth rate for a given Bond number and spherical mode number, which requires solving another eigenvalue problem as follows.

Equation (29) can be rewritten as

$$\frac{l(l-m)}{2l-1}\eta_{l-1}^{m} - \frac{l(l-1)(l+2)}{Bo}\eta_{l}^{m} + \frac{l(l+m+1)}{2l+3}\eta_{l+1}^{m} = \hat{\zeta}^2\eta_{l}^{m}, l = 2,3,\ldots, \qquad (31)$$

in which $\hat{\zeta}^2$ can be considered as the eigenvalue of a tri-diagonal coefficient matrix **S**. Similar to that for **M**, the eigenvalue problem for **S** was also solved numerically by truncating the coefficient matrix above $S_{N,N}$ with a sufficiently large value of N. For a given Bo, the negative value of $\hat{\zeta}^2(l,m,Bo)$ results in a virtual growth rate, indicating the disturbance of corresponding spherical modes (l, m) is in a stable oscillatory state. In this study, we are only interested in the positive value of $\hat{\zeta}^2$ and its corresponding modes. The negative real root $\hat{\zeta} = -|\hat{\zeta}|$ indicates the exponential growth of the initial

disturbance. The most-unstable mode is the one with the largest positive value of $\hat{\zeta}^2$.

The methodology to calculate the value of $\hat{\zeta}^2$ and determine the most-unstable mode is illustrated in the following example of Bo = 50. As discussed above, the disturbance of meridional mode number m larger than 3 is not excited because Bo = 50 considered here is smaller than the lowest $(Bo_{cr})_i$ = 53.42 for m = 4. From Table 1 we can see that there are seven possibly excited modes (two for each case of m = 0, 1, 2 and one for the case of m = 3) for Bo < 50, among which the excitable modes and the mode possessing the largest growth rate are still unknow. Table 2 gives the first ten eigenvalues $\hat{\zeta}^2$ for m = 0, 1, 2, 3 and 4 at Bo = 50. It can be seen that the seven possibly excited spherical modes as indicated in Table 1 are (2, 0), (4, 0), (2, 1), (4, 1), (2, 2), (4, 2) and (4, 3), respectively. Table 2 shows that for the case of Bo = 50, the growth rate of the zonal mode l = 4 overwhelms that of l = 2, and the most-unstable mode is (4, 0) with the largest growth rate $|\hat{\zeta}| = \sqrt{1.88} = 1.37$. Following the same procedures, we can calculate the growth rate and determine the most-unstable modes for other Bond numbers (see Table 3 and Table 4 as another two examples).

Table 2 The first ten eigenvalues $\hat{\zeta}^2$ for m = 0, 1, 2, 3 and 4 at Bo = 50. The italic bold values represent the unstable modes possibly excited.

	$m = 0$	$m = 1$	$m = 2$	$m = 3$	$m = 4$
$l = 2$	***0.47***	***0.42***	***0.26***	N	N
$l = 3$	-1.02	-1.01	-0.96	-0.62	N
$l = 4$	***1.88***	***1.78***	***1.47***	***0.84***	-0.17
$l = 5$	-2.64	-2.61	-2.50	-2.31	-2.03
$l = 6$	-4.71	-4.69	-4.61	-4.48	-4.31

$l = 7$	-7.50	-7.48	-7.43	-7.35	-7.23
$l = 8$	-11.16	-11.15	-11.11	-11.05	-10.96
$l = 9$	-15.81	-15.80	-15.77	-15.73	-15.67
$l = 10$	-21.58	-21.57	-21.55	-21.52	-21.47
$l = 11$	-28.58	-28.57	-28.56	-28.53	-28.50

Table 3 The first ten eigenvalues $\hat{\zeta}^2$ for $m = 0$, 1, 2, 3, 4, 5 and 6 at $Bo = 100$. The italic bold values represent the unstable modes possibly excited.

	$m = 0$	$m = 1$	$m = 2$	$m = 3$	$m = 4$	$m = 5$	$m = 6$
$l = 2$	***0.51***	***0.47***	***0.34***	N	N	N	N
$l = 3$	-0.76	-0.75	-0.71	-0.34	N	N	N
$l = 4$	***1.73***	***1.66***	***1.42***	***0.92***	***0.14***	N	N
$l = 5$	-2.07	-2.04	-1.92	-1.69	-1.37	***0.70***	N
$l = 6$	***2.98***	***2.90***	***2.66***	***2.23***	***1.59***	-0.96	-0.49
$l = 7$	-3.58	-3.55	-3.45	-3.29	-3.06	-2.78	-2.44
$l = 8$	-5.46	-5.44	-5.37	-5.25	-5.09	-4.88	-4.63
$l = 9$	-7.82	-7.80	-7.75	-7.67	-7.55	-7.39	-7.21
$l = 10$	-10.73	-10.71	-10.68	-10.61	-10.52	-10.40	-10.26
$l = 11$	-14.24	-14.23	-14.20	-14.15	-14.08	-13.99	-13.88

Table 4 The first ten eigenvalues $\hat{\zeta}^2$ for $m = 0$, 1, 2, 3, 4, 5, 6, 7 and 8 at $Bo = 200$. The italic bold values represent the unstable modes possibly excited.

	$m = 0$	$m = 1$	$m = 2$	$m = 3$	$m = 4$	$m = 5$	$m = 6$	$m = 7$	$m = 8$
$l = 2$	-0.04	-0.06	-0.09	N	N	N	N	N	N
$l = 3$	***1.05***	***1.01***	***0.85***	***0.37***	N	N	N	N	N
$l = 4$	-1.16	-1.14	-1.05	-0.74	-0.34	N	N	N	N
$l = 5$	***2.13***	***2.07***	***1.87***	***1.49***	***0.92***	***0.15***	N	N	N
$l = 6$	-2.31	-2.27	-2.16	-1.94	-1.65	-1.27	***0.71***	N	N
$l = 7$	***3.27***	***3.21***	***3.02***	***2.69***	***2.20***	***1.55***	-0.84	-0.35	N
$l = 8$	-3.60	-3.57	-3.47	-3.31	-3.09	-2.81	***2.25***	***1.32***	***0.19***

l = 9	***4.53***	***4.47***	***4.30***	***4.00***	***3.56***	***2.99***	-2.47	-2.08	-1.65
l = 10	-5.13	-5.11	-5.03	-4.91	-4.74	-4.52	-4.25	-3.95	-3.60
l = 11	-6.95	-6.93	-6.87	-6.77	-6.64	-6.47	-6.26	-6.01	-5.74

One interesting result we obtained after repeating the above-mentioned procedure for other Bond numbers is that the most-unstable mode with the largest growth rate always corresponds to m = 0, although the corresponding zonal mode l increases with Bo accordingly. For example, the most-unstable modes for the cases of Bo = 100 and Bo = 200 are (6, 0) and (9, 0), respectively. In fact, similar to the procedure to determine the critical Bond numbers for neutral growth, we can obtain the minimum Bond numbers required to reach specified growth rates for different meridional modes from Eq. (29), which are depicted in Fig. 2. It shows that for a given Bond number, the meridional mode m = 0 always possesses the largest growth rate. This is consistent with the observation in experiments at initial stage when the linear theory is valid **[32-34]**. As the Bond number increases, the difference in growth rate between different meridional modes decreases and, as will be discussed in §5, m has no effects on the growth rate in the large-mode number limit.

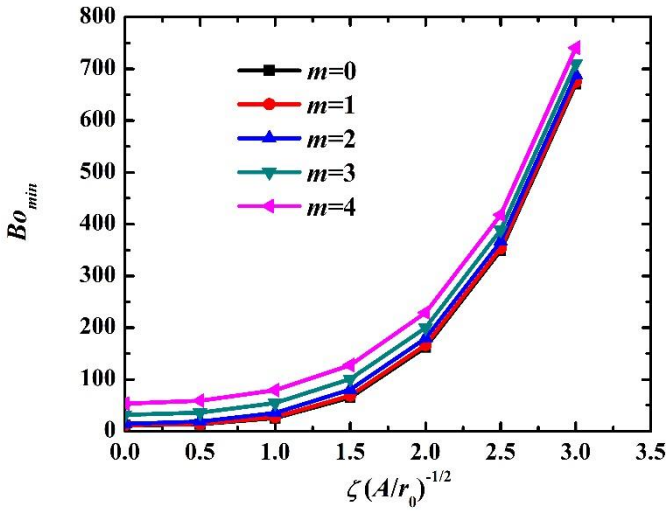

Fig. 2 The minimum Bond numbers required to reach different growth rates for meridional modes m = 0, 1, 2, 3 and 4.

5. Large-mode number limit

The Bond number of the droplet in aircraft and automotive engine conditions can reach as large as $O(10^5)$, rendering the neutral and dominant mode numbers are very large **[23]**. It is of great interest to study the spherical R-T instability for the limit case of $l \gg 1$, in which the spherical harmonic $Y_l^m(\theta,\varphi)$ oscillates much "faster" than the spatial variation (i.e., $\cos\theta$) of external acceleration along the polar direction. In other words, θ can be recognized as a quickly varying variable for the interfacial displacement change and a slowly varying variable for the acceleration. As a result, each spherical harmonic in this limiting case can be treated separately instead of solving the eigenvalue problem for the coefficient matrix of difference equations like (28), (29) and (30), which can give an explicit dispersion relation of ζ as a function of l.

In the limiting case $l \gg 1$, the asymptotic expansion of the Bessel function **[35]** gives $Q_l(x) = J_{l+1}(x)/J_l(x) \approx x/2l$. Because the different modes of spherical harmonics are decoupled in space in this limiting case, the recursion relation (28) can reduce to

$$\tilde{\zeta}^2 - 2Ohl^2\tilde{\zeta} + \left(l^3 - lBo\cos\theta\right) = 0 \tag{32}$$

for the case of $\rho_2 \ll \rho_1$, where $\tilde{\zeta} = \zeta/\sqrt{\alpha/\rho_1 r_0^3}$ is the dimensionless growth rate and $Oh = \mu_1/\sqrt{\rho_1 \alpha r_0}$ is the Ohnesorge number which measures the ratio of viscous force to capillary force. Solving the quadratic equation (32) gives the explicit dispersion relation:

$$\tilde{\zeta} = Ohl^2 - \sqrt{Oh^2 l^4 + lBo\cos\theta - l^3}\,. \tag{33}$$

We have neglected the positive solution of $\tilde{\zeta}$, which leads to absolute stable states of the external disturbance. It is of interest to find that the growth rate no longer depends on the meridional mode number *m* for $l \gg 1$.

Figure 3 shows the effect of polar angle θ on $\tilde{\zeta}$ for a given condition of $Bo = 10^4$ and $Oh = 0.01$ as an example. The magnitude of growth rate is increased with the decrease of θ, indicating that the unstable wave grows fastest at the stagnation point in the windward of the liquid droplet for the same mode. Furthermore, the range of the unstable modes shrinks and the most-unstable mode number decreases as θ increases. This suggests that, for each mode number *l*, there exists a critical polar angle $\theta_c(l)$, and that no instability occurs on the surface beyond the critical angle. $\theta_c(l)$ can be evaluated as $\theta_c(l) = \arccos\left(l^2/Bo\right)$ from Eq. (33). The leeward of the liquid droplet is unconditionally stable because θ larger than $\pi/2$ always leads to $\mathrm{Re}\left(\tilde{\zeta}\right) > 0$.

For any *Oh* number, the neutral stability condition $\tilde{\zeta} = 0$ in Eq. (33) always leads to $lBo\cos\theta - l^3 = 0$, solving which gives $l = \sqrt{Bo\cos\theta}$, with maximum value of $l_c = \sqrt{Bo}$ at $\theta = 0$. Any disturbance of mode $l > l_c$ shall be stabilized, which is in accordance with the result obtained by Harper et al. **[23]**.

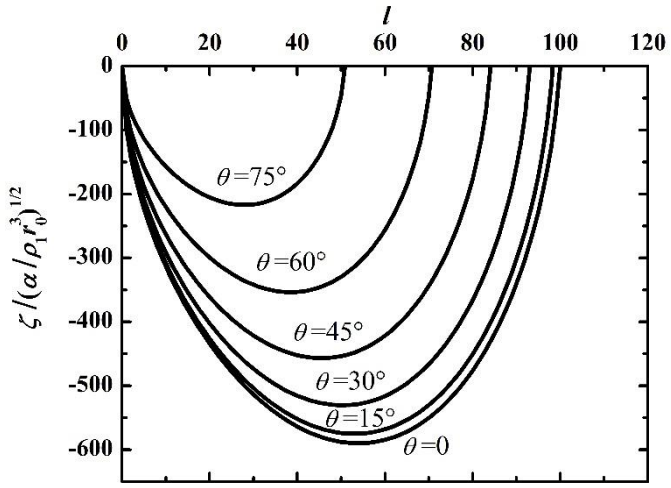

Fig. 3 Dimensionless growth rate $\tilde{\zeta} = \zeta \Big/ \sqrt{\alpha/\rho_1 r_0^3}$ as a function of mode number l for Bo = 10^4 and Oh = 0.01 with the polar angle θ = 0, 15°, 30°, 45°, 60° and 75°.

Figure 4 shows the effect of Ohnesorge number Oh on $\tilde{\zeta}$ for a given condition of Bo = 10^4 and θ = 0. Although the viscosity has no influence on the cut-off mode number l_c, as indicated above, the magnitude of growth rate decreases as Oh increases due to the viscous dissipation. In addition, the decrease of the most-unstable mode number with the increase of Oh implies that the higher liquid viscosity would give rise to larger sizes of droplets after atomization.

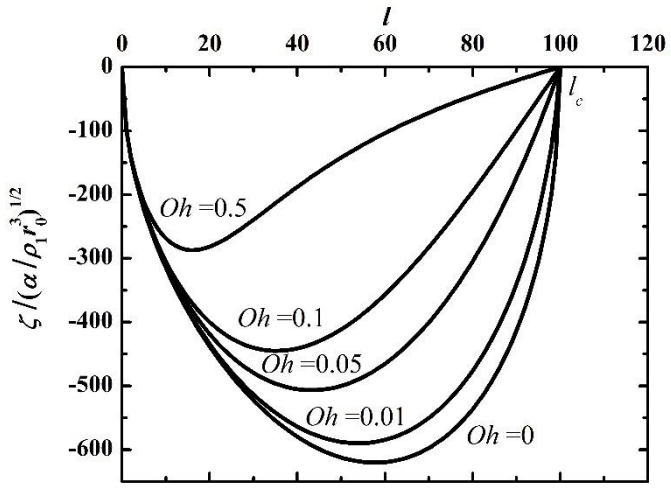

Fig. 4 Dimensionless growth rate $\tilde{\zeta} = \zeta \Big/ \sqrt{\alpha/\rho_1 r_0^3}$ as a function of mode number l for Bo = 10^4 and θ = 0 with Oh = 0, 0.01, 0.05, 0.1 and 0.5.

The cut-off mode number l_c suggests that there exists a critical diameter d_c,

smaller than which the liquid droplet is unconditionally stable to the initial disturbance of any kind. Assuming the windward of the droplet as a flat surface, Joseph et al. **[10]** suggested a criterion $d_c = \lambda_c = 2\pi\sqrt{\alpha/\rho_1 A}$, where λ_c is the cut-off wavelength for the planar R-T instability. Considering the spherical shape of the liquid droplet, we shall first determine the wavelength corresponding to l_c on the windward surface. Since the dispersion relation does not relate to m for $l \gg 1$, without loss of generality, we consider the case of $m = 0$, in which $Y_l^0(\theta,\varphi) = P_l(\cos\theta)$. Then the wavelength around $\theta = 0$, where l_c maximizes its value, can be defined as $\lambda_c = 2r_0\theta_m$, where θ_m is the polar angle corresponding to the first minimum (trough) of $P_l(\cos\theta)$. Using the approximation expression of $P_l(\cos\theta)$ at $l \gg 1$ **[35]**,

$$P_l(\cos\theta) = \sqrt{2/(\pi l \sin\theta)}\sin\left[(l+1/2)\theta + \pi/4\right]\left[1 + O\left(l^{-1}\right)\right], \tag{34}$$

we can obtain

$$\theta_m \approx 5\pi/(4l_c) \tag{35}$$

and

$$d_c = \lambda_c = 2r_0\theta_m \approx 5\pi r_0/\left(2\sqrt{Bo}\right) = 2.5\pi\sqrt{\alpha/\rho_1 A}\,. \tag{36}$$

This result is similar as that for the flat surface but with a coefficient of larger value, which reflects the influence of the spherical shape of the liquid droplet.

The most-unstable mode occurring at $\theta = 0$ can be derived from Eq. (33) as

$$l_m = \sqrt{\frac{Bo}{3}}\left[1 - \frac{2^{3/2}3^{3/4}Bo^{1/4}}{9}Oh\right], \tag{37}$$

with which the growth rate reaches its maximum magnitude of

$$\tilde{\zeta}_m = -\sqrt{2}\left(\frac{Bo}{3}\right)^{3/4}\left[1-\frac{\sqrt{2}}{2}Oh\left(\frac{Bo}{3}\right)^{1/4}\right]. \quad (38)$$

The surface waves corresponding to the most-unstable mode would dominate over others and increase their amplitudes until atomization occurs. Although the most-unstable mode derived here by linear analysis is only strictly valid for small deformation, the mode is believed to continue to lead in growth when the surface deformation becomes large **[36]**. Given the most-unstable mode and its corresponding growth rate, we can roughly predict the dominant size of droplets and breakup time for a given *Bo* and *Oh*, which are useful information to construct practical atomization models for the simulation of spray combustion.

6. Concluding Remarks

As one of the primary mechanisms for droplet secondary atomization in spray combustion, the R-T instability for a viscous spherical droplet in high-speed gas stream with arbitrary disturbances was theoretically investigated by a linear analysis. Being more general than that obtained in the previous studies, a recursion dispersion relation coupling different spherical modes was derived to compute the growth rate of the R-T waves. In addition to the zonal mode number *l*, the coefficients of the recursion relation are also the function of the meridional mode number *m*.

In the limiting case of negligible droplet viscosity, a set of critical Bond numbers $(Bo_{cr})_i$ corresponding to the neutral stability state were obtained by solving an eigenvalue problem derived from the recursion relation. The results show that $(Bo_{cr})_i$

increases as the meridional mode number *m* increases, and the global minimum value is $(Bo_{cr})_{min}$=11.22, below which no instability occurs on the spherical surface. The growth rates for a given Bond number can be computed by solving another eigenvalue problem derived from the recursion relation, from which the most-unstable mode can be determined.

In the limiting case of large droplet acceleration rendering the large-mode number approximation, different modes are asymptotically decoupled and each spherical harmonic can be treated separately, which gives an explicit dispersion relation. The predicted critical diameter of droplets being stable to any disturbance is 25% larger than that reported in the previous studies by approximating the droplet surface to be flat, indicating that the influence of the spherical shape on the R-T instability is significant. The most-unstable mode and corresponding growth rate as explicit functions of *Bo* and *Oh* were deduced. The results gained in the present study are useful to construct the atomization model for spray combustion simulation. An important future work that would complement the present one is to study the influence of simultaneous K-H instability on the R-T instability.

Acknowledgement

The work in the Beijing Institute of Technology was supported by the National Natural Science Foundation of China (Grant No.: 51606010) and Beijing Natural Science Foundation (Grant No.:3174055). The work in the Hong Kong Polytechnic

University was supported by the Hong Kong Research Grants Council/General Research Fund (PolyU 152217/14E and PolyU 152651/16E).

Reference

[1] J.E. Dec. Advanced compression-ignition engines-understanding the in-cylinder processes. Proc Combust Inst. 32 (2009) 2727-42.
[2] R.D. Reitz. Directions in internal combustion engine research. Combust Flame. 160 (2013) 1-8.
[3] J. Shinjo, A. Umemura. Detailed simulation of primary atomization mechanisms in Diesel jet sprays (isolated identification of liquid jet tip effects). Proc Combust Inst. 33 (2011) 2089-97.
[4] D. Guildenbecher, C. Lopez-Rivera, P. Sojka. Secondary atomization. Exp Fluids. 46 (2009) 371-402.
[5] Z. Wang, X. Dai, F. Li, Y. Li, C.-F. Lee, H. Wu, et al. Nozzle internal flow and spray primary breakup with the application of closely coupled split injection strategy. Fuel. 228 (2018) 187-96.
[6] L.P. Hsiang, G.M. Faeth. Near-limit drop deformation and secondary breakup. Int J Multiph Flow. 18 (1992) 635-52.
[7] L.P. Hsiang, G.M. Faeth. Drop properties after secondary breakup. Int J Multiph Flow. 19 (1993) 721-35.
[8] S. Hwang, Z. Liu, R.D. Reitz. Breakup mechanisms and drag coefficients of high-speed vaporizing liquid drops. Atomization Sprays. 6 (1996) 353-76.
[9] Z. Zhang, P. Zhang. Cross-impingement and combustion of sprays in high-pressure chamber and opposed-piston compression ignition engine. Applied Thermal Engineering. 144 (2018) 137-46.
[10] D.D. Joseph, J. Belanger, G.S. Beavers. Breakup of a liquid drop suddenly exposed to a high-speed airstream. Int J Multiph Flow. 25 (1999) 1263-303.
[11] C.S. Lee, R.D. Reitz. Effect of liquid properties on the breakup mechanism of high-speed liquid drops. Atomization Sprays. 11 (2001) 1-19.
[12] W.D. Arnett, J.N. Bahcall, R.P. Kirshner, S.E. Woosley. Supernova 1987A. Annu Rev Astro Astrophys. 27 (1989) 629-700.
[13] C.H. Miller, W. Tang, M.A. Finney, S.S. McAllister, J.M. Forthofer, M.J. Gollner. An investigation of coherent structures in laminar boundary layer flames. Combust Flame. 181 (2017) 123-35.
[14] P. Ramaprabhu, M. Andrews. Experimental investigation of Rayleigh-Taylor mixing at small Atwood numbers. J Fluid Mech. 502 (2004) 233-71.
[15] L. Rayleigh. Investigation of the character of the equilibrium of an incompressible heavy fluid of variable density. Proc London Math Soc. 14 (1883) 170-7.
[16] G.I. Taylor. The instability of liquid surfaces when accelerated in a direction

perpendicular to their planes. I. Proc R Soc London Ser A. 201 (1950) 192-6.
[17] R. Bellman, R.H. Pennington. Effects of surface tension and viscosity on Taylor instability. Quart J Appl Math. 12 (1954) 151.
[18] J.P. McGarry, K.A. Ahmed. Flame-turbulence interaction of laminar premixed deflagrated flames. Combust Flame. 176 (2017) 439-50.
[19] P. Ramaprabhu, G. Dimonte, M. Andrews. A numerical study of the influence of initial perturbations on the turbulent Rayleigh-Taylor instability. J Fluid Mech. 536 (2005) 285-320.
[20] K.O. Mikaelian. Rayleigh-Taylor and Richtmyer-Meshkov instabilities and mixing in stratified spherical shells. Phys Rev A. 42 (1990) 3400-20.
[21] M.S. Plesset, A. Prosperetti. Bubble dynamics and cavitation. Annu Rev Fluid Mech. 9 (1977) 145-85.
[22] G. Terrones, M.D. Carrara. Rayleigh-Taylor instability at spherical interfaces between viscous fluids: Fluid/vacuum interface. Phys Fluids. 27 (2015) 054105.
[23] E.Y. Harper, G.W. Grube, I.D. Chang. On the breakup of accelerating liquid drops. J Fluid Mech. 52 (1972) 565-91.
[24] P.G. Simpkins, E.L. Bales. Water-drop response to sudden accelerations. J Fluid Mech. 55 (1972) 629-39.
[25] J.W. Miles. On the generation of surface waves by shear flows Part 3. Kelvin-Helmholtz instability. J Fluid Mech. 6 (1959) 583-98.
[26] H. Lamb. Hydrodynamics. Cambridge University Press1932.
[27] S. Chandrasekhar. Hydrodynamic and Hydromagnetic Stability. Oxford: Clarendon Press1961.
[28] A.H.E. Adou, L.S. Tuckerman. Faraday instability on a sphere: Floquet analysis. J Fluid Mech. 805 (2016) 591-610.
[29] K. Kumar, L.S. Tuckerman. Parametric instability of the interface between two fluids. J Fluid Mech. 279 (1994) 49-68.
[30] T. Donnelly, J. Hogan, A. Mugler, N. Schommer, M. Schubmehl, A.J. Bernoff, et al. An experimental study of micron-scale droplet aerosols produced via ultrasonic atomization. Phys Fluids 16 (2004) 2843-51.
[31] R.J. Lang. Ultrasonic atomization of liquids. The journal of the acoustical society of America. 34 (1962) 6-8.
[32] F. Liu, N. Kang, Y. Li, Q. Wu. Experimental investigation on the atomization of a spherical droplet induced by Faraday instability. Experimental Thermal and Fluid Science. 100 (2019) 311-8.
[33] F. Liu, N. Kang, Y. Li, Q. Wu. Experimental investigation on the spray characteristics of a droplet under sinusoidal inertial force. Fuel. 226 (2018) 156-62.
[34] A. James, B. Vukasinovic, M.K. Smith, A. Glezer. Vibration-induced drop atomization and bursting. J Fluid Mech. 476 (2003) 1-28.
[35] E.T. Copson. Asymptotic expansions. Cambridge University Press2004.
[36] M.S. Plesset, C.G. Whipple. Viscous effects in Rayleigh-Taylor instability. Phys Fluids. 17 (1974) 1-7.